Materials and Design 160 (2018) 828–835

Contents lists available at ScienceDirect

Materials and Design

journal homepage: www.elsevier.com/locate/matdes

Characterization of innovative rotary swaged Cu-Al clad composite wire conductors

Radim Kocich [a], Lenka Kunčická [b,*], Petr Král [b], Pavel Strunz [c]

[a] VŠB – Technical University of Ostrava, 17. Listopadu 15, Ostrava 8, Czech Republic
[b] Institute of Physics of Materials, ASCR, 61662 Brno, Czech Republic
[c] Nuclear Physics Institute, ASCR, Řež, 130, Husinec, Czech Republic

HIGHLIGHTS

- Clad composite wires with 5 mm diameter were produced via rotary swaging.
- Composite structures featured ultra-fine grains.
- Room temperature swaging induced neglectable intermetallics development.
- Work hardening increased ultimate tensile strength to approx. 250 MPa.
- Structure restoration and refinement increased electric conductivity.

GRAPHICAL ABSTRACT

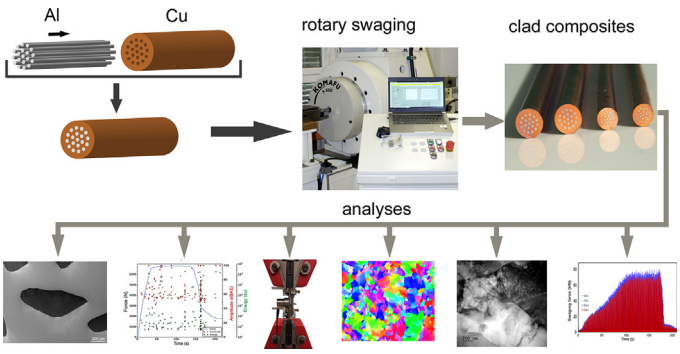

ARTICLE INFO

Article history:
Received 15 August 2018
Received in revised form 3 October 2018
Accepted 15 October 2018
Available online 17 October 2018

Keywords:
Clad composite
Rotary swaging
Electrical resistivity
Scanning electron microscopy
Interfaces
Mechanical properties

ABSTRACT

Cu/Al composites are perspective for applications in a wide range of industrial and commercial branches, from transportation to elecatrotechnics. This study focuses on Cu/Al clad composite wires with 5 mm in diameter featuring unique sequencing produced via the technology of rotary swaging at the processing temperatures of 20 °C and 250 °C. During the swaging process, we continuously acquired samples for investigations and used our own KOMAFU S600 system for dynamic detection of swaging forces. The composite wires subjected to electrical resistivity measurement were further analysed via electron microscopy, neutron diffraction, and mechanical testing. The results showed that both the total imposed strain (swaging degree) and swaging temperature influenced the investigated parameters non-negligibly. The samples subjected to high reduction ratios (swaging degree > 3) at the temperature of 250 °C exhibited formation of intermetallics at the interfaces, which deteriorated the electric conductivity. However, the conductivity was also affected by structural phenomena, such as work hardening, texture development, dislocations density, and recrystallization. All the final 5 mm samples exhibited sufficient bonding of both the components and recrystallized ultra-fine grained structures providing them with the ultimate tensile strength of >200 MPa.

1. Introduction

Hybrid materials, heterogeneous laminates, and clad composites featuring the possibility to achieve optimized combinations of properties represent innovative materials consisting of two or more different

* Corresponding author.
E-mail address: lenka.kuncicka@vsb.cz (L. Kunčická).

https://doi.org/10.1016/j.matdes.2018.10.027
0264-1275/

(metallic) materials bond together at adjoining interfaces [1–4]. These materials are gaining increasing popularity in the aeronautics, automotive, marine industry, thermal engineering, electrotechnics, medicine, and many more industrial and commercial branches [5–10].

Among the most popular metal-metal composite systems is the Al/Cu one. Beside other advantages, both the metals have wide applicability as electric conductors. Most of the electro-conductive wires in households and vehicles are made from copper, which is relatively expensive and heavy. The electric conductors in power distribution systems usually consist of aluminium wires strengthened with steel cores, the electric current passing through which tends to generate magnetic field around the conductors and cause undesirable energy loses. By these reasons, alternatives reducing the disadvantages and side effects of the electric transport are researched.

The design process of clad composites and hybrid materials involves not only selection of suitable materials and their stacking sequences, but also optimization of the processing conditions. Production of a layered clad composite without negatively influencing the physical properties, especially the electrical conductivity, is a real challenge since they can significantly be deteriorated by (local) temperature increase and the consequent development of various forms of intermetallic phases at the interfaces [11]. By this reason, the typically used welding technologies are disadvantageous. On the other hand, processing technologies involving intensive plastic deformation ensuring bonding of the components by introducing shear strain, performed preferably under cold conditions, have been shown to be advantageous for production of clad composites and hybrid materials with favourable properties [1,4,12–20]. Production under cold conditions supports significant increase in strength, but also invokes decrease in material formability (gradual exhaustion of plasticity) and increase in power demands. Post-production heat treatment can be advantageous when optimized, however, it can significantly deteriorate the components bonding strength (depending also on the used metals) [1,21].

The objective of this study was to produce industrially applicable Cu/Al composite wires with 5 mm diameter and favourable electric conductivity and advantageous mechanical properties. For this purpose, we designed unique sequencing and geometry of the original material. The herein presented investigations focused on the composites behaviour and properties after swaging under various processing conditions.

2. Materials and methods

The used materials were commercially pure (CP) electro-conductive (EC) copper (0.002% O, 0.015% P, 0.002% Zn, balance Cu), and CP EC aluminium (0.20% Si, 0.25% Fe, 0.05% Cu, balance Al). The initial diameter of the Cu sheath was 30 mm, the Al wires diameters were 3 mm each, and the volume ratio of Al and Cu within the composites was 81:19 (Fig. 1). In the following text, the examined wires within the composites are categorized as the axial wire, the inter-layer wires and the outer-layer wires (cross-sectional cut).

The Cu/Al clad composites were produced via rotary swaging (RS), a versatile processing technology reducing the material via a repeated action of rotating swaging dies (Fig. 1) suitable also for production of gradient materials, inducing progressive grain refinement, enhancing mechanical and utility properties and ensuring exceptional final surface quality [8,22–24]. Based on previous research [1,25,26], RS was performed at two different temperatures - room temperature for composite *A* and 250 °C for composite *B*.

Both the *A* and *B* composites were swaged to the final diameter of 5 mm, however, samples for subsequent analyses were acquired also after swaging to 10 mm, 7.5 mm, and 6 mm. The reduction ratio (deformation degree) in the individual swaging passes depicted in Table 1 was computed using the $\varphi = \ln(S_0/S_n)$ relation, where S_0, S_n were the original and final cross-sectional areas, respectively. In order to be able to evaluate and compare the behaviour of the two composites during swaging, we implemented our own patented Komafu S600 system for dynamic detection of swaging forces.

700 mm long swaged composite samples of the investigated diameters were subjected to electrical conductivity measurements performed at room temperature. The measurements were carried out using a Metex MS-9170 device, the electric voltage *U* by which was determined. Subsequently, the specific electrical resistivity ρ was calculated using the $\rho = U \cdot S/I \cdot L$ formula, where *S* was the composite cross-sectional area, *I* was current and *L* was the measured composite length. The composites mechanical properties were investigated via room temperature tensile testing. The tests were performed at room temperature using a Testometric M500-50CT machine. The composite *A* and composite *B* tensile tests specimens with the diameters of 10 mm, 7.5 mm, 6 mm and 5 mm were 150 mm long and the strain rate was $1.5 \times 10^{-3}\ s^{-1}$.

Detailed analyses of the swaged composites structures and the Cu/Al interfaces were performed via scanning electron microscopy (SEM), Electron Backscatter Diffraction (EBSD), energy dispersive spectroscopy (EDX), and transmission electron microscopy (TEM). Preparations of the samples for SEM, EBSD, and EDX analyses were carried out by grinding on SiC papers and electrolytical polishing. SEM investigations were carried out using a Tescan Lyra 3 FIB/SEM microscope. EBSD scanning was performed on samples of composites transversal sections using a JEOL FESEM 7000F device with an EDAX DigiView High Resolution Camera. The EBSD analyses were performed on samples tilted by 70° with the scan steps of 40 nm and the accelerating voltage of 20 kV. EDX observations of the intermetallics were performed with the accelerating voltage of 10 kV in order to minimise the noise from the surrounding material. The TEM samples were prepared by a twin-jet electropolishing machine and subsequently analysed using a Jeol 2100F TEM microscope operating at 200 kV.

Last but not least, the investigations were supplemented with neutron diffraction measurements analysing the widths of diffraction peaks (FWHM) pointing to dislocation density and structure recovery. The neutron diffraction is also advantageous for determination of possible residual stress in the structure. The measurements were performed using the TKSN-400 neutron diffractometer with Si monochromator installed in ASCR, Řež. The parameters used for the measurements were – pixel size of 0.718 mm, specimen to detector distance 13,560 mm, $\ddot{e}_1 = 2.42$ Å, $\lambda_2 = 1.21$ Å. The lattice parameters of the composite components were a = 3.6149 Å for Cu and a = 4.0490 Å for Al. For both the metals, the measurements were carried out along the central line on samples cross-sections (perpendicular to the swaging axis).

3. Results and discussion

3.1. Deformation behaviour

As evident from the graphically adjusted SEM-BSE scans depicted in Fig. 2, the Al wires within 10 mm composite *A* were circular and exhibited uniform distribution across the composite cross-section. On the other hand, the Al wires cross-sectional circularity diminished for

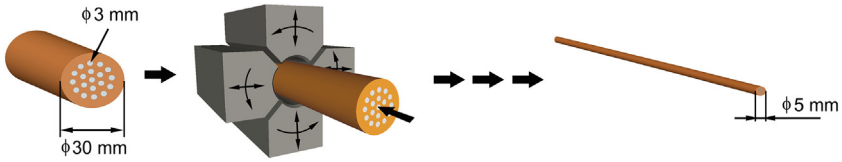

Fig. 1. Schematics of rotary swaging technology; rotating dies and original and final materials.

Table 1
Reduction ratios for individual swaging passes.

RS pass number	1	2	3	4	5	6	7	8	9	10	11
Total deformation degree φ	0.36	0.81	1.08	1.39	1.75	2.20	2.77	3.03	3.22	3.39	3.58

10 mm composite *B*. The centripetal rotary movement of the dies affects the swaged material with force consisting of normal, as well as radial component, which introduces shear strain imparting the material the tendency towards vortex-like flow [27].

This was notable the more the higher was the reduction ratio (Fig. 2). For 10 mm composite *B*, the influence of the radial plastic flow was especially evident on the outer-layer wires. However, with continuing swaging, the radial force component also affected the inter-layer wires and the axial wire, the cross-sections of which exhibited an increasing tendency to deform.

The material behaviour and plastic flow during swaging are affected not only by the swaging force, but also by the total imposed strain, and swaging temperature (however inhomogeneously from surface towards the axis [22,28]). Although originally having identical cross-sectional areas, the total cross-sectional area of the Al wires slightly decreased with continuing swaging for both the composites (Table 2). This phenomenon was caused by the influence of the radial plastic flow supported by the vortex flow tendency and the effect of free ends [8]. As reported before, for clad composite materials consisting of metals featuring different properties, the plastic deformation primarily affects the material with lower flow stress (aluminium) [1,25]. The higher swaging temperature most probably imparted the occurrence of dynamic softening and subsequently decreased the flow stress (as also commented below) which facilitated the plastic flow in both the radial and axial directions, however, increased temperature can support the development of intermetallics on the interfaces of the components which can possibly deteriorate the mechanical and utility properties of the final product [1,29].

Scanning and transmission electron microscopy analyses of the interfaces revealed no significant occurrence of intermetallics within the 10 mm and 7.5 mm composites *A*. However, local island-form intermetallics started to develop within 7.5 mm composite *B* samples (Fig. 3a and b depict the interfaces of 7.5 mm composites *A* and *B*, respectively). As regards 6 mm and 5 mm samples, composite *A* featured a scarce local presence of intermetallic phases on the very Cu/Al interfaces. An example of the 6 mm composite B interface can be seen in Fig. 3c. The detected compounds consisted of a mixture of Al_2Cu_3 and Al_4Cu_9 phases, which have previously been reported to develop in a small extent during local heating caused by plastic deformation [29]. Nevertheless, the vast majority of composite *A* Cu/Al interfaces exhibited perfect coupling of both the metals. A detailed analysis of 5 mm composite *A* performed by TEM proved perfect connection of the two metals; Fig. 3d and e show that the blending zone of the two metals was only a few tens of nanometres wide.

On the other hand, the presence of intermetallics was detected in both the 6 mm and 5 mm composite *B* samples, the interfaces of which are depicted in Fig. 3f and g, respectively. Together with Al_2Cu_3 and Al_4Cu_9, this composite also exhibited the formation of AlCu and Al_2Cu phases.

3.2. Swaging forces

The evaluation of the swaging forces was performed via comparison of the envelop curves created for all the recorded individual swaging strokes for each pass (example for the first swaging pass shown in Fig. 4a). At the beginning of the swaging technology (for approx. half of the passes), the maximum swaging force slightly decreased between the individual passes. In this stage of processing, the total strain imposed into the composite was not sufficient enough to induce significant work hardening. Moreover, the material exhibited notable axial flow when unconstrained by the swaged ends [8].

The work hardening effect and the effect of swaged ends increased with increasing total imposed strain. They supported composite strengthening and aggravated the plastic flow, while significant reduction in diameter and deformation heat development supported composite softening and flow stress decrease. The mutual effect of these phenomena resulted in more or less comparable (steady) swaging forces values during subsequent stages of the swaging technology (Fig. 4b depicts the forces for the 5th swaging pass). The joint effect of the increased total imposed strain and decreased work-piece diameter in these passes enabled the imposed strain to affect also the internal layers of the processed composite, which facilitated the axial as well as radial plastic flow (as also discussed in the foregoing section) and resulted in the generally lower swaging force values (the maximum force

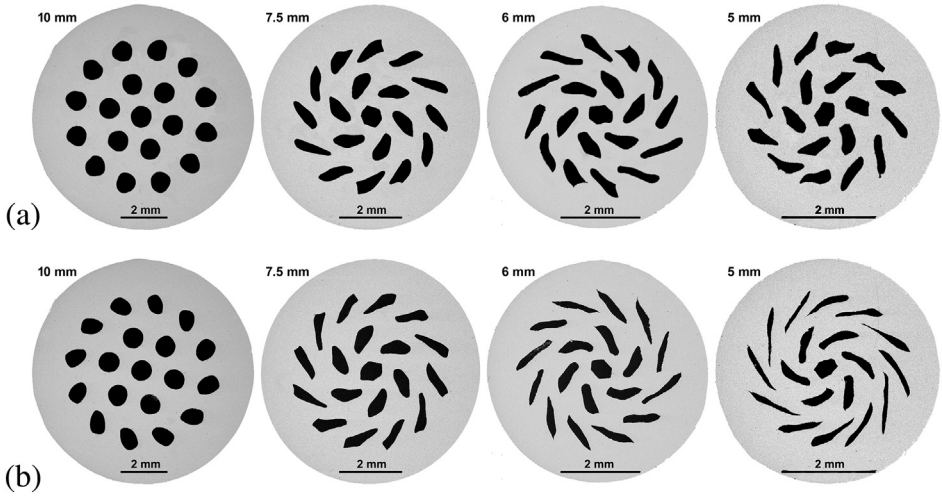

Fig. 2. Cross sections of individual swaged composites: A (a), B (b).

Table 2
Total areas of Al wires within perpendicular cross-sections of composite samples.

Composite type	*A*				*B*			
Diameter (mm)	10	7.5	6	5	10	7.5	6	5
Cross-sectional area of Al (%)	16	15	14	13	15	15	13	12

was approx. twice as high for the first pass than for the fifth one for both the composites). The comparison of the swaging forces developments shows that higher deformation forces were recorded for composite *A* in all the swaging passes, which corresponds to the afore mentioned facilitated plastic flow in case of composite *B*.

3.3. Mechanical properties

The mechanical properties examined via tensile testing showed higher ultimate tensile strength (UTS) for composites *A* (comparison of identical composite diameters). However, composite *B* exhibited better

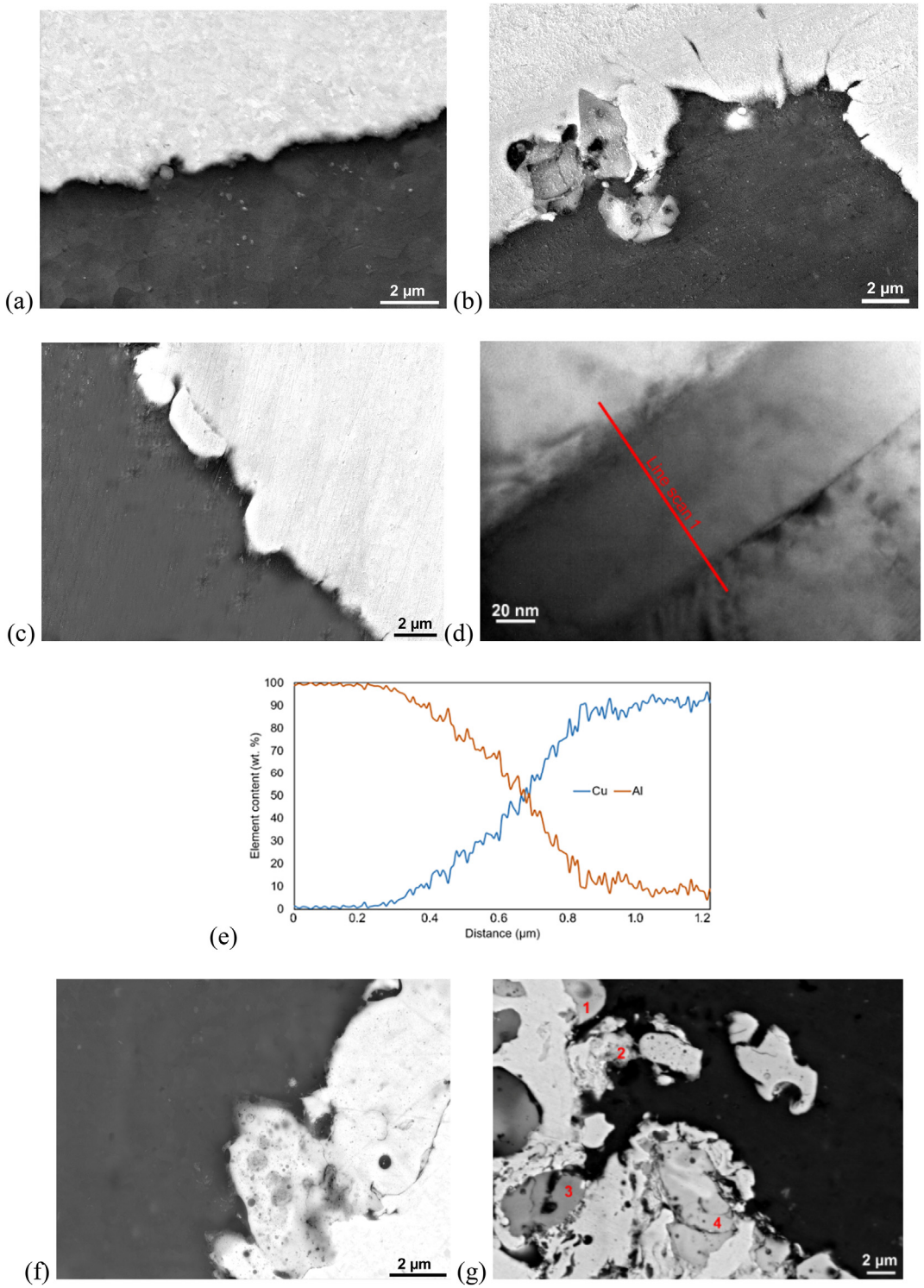

Fig. 3. SEM image of 7.5 mm composite A (a); SEM image of 7.5 mm composite B (b); SEM image of 6 mm composite A (c); TEM image of 5 mm composite A (d); element composition data measured via Line scan 1 depicted in panel d (e); intermetallic phases within 6 mm composite B (f); intermetallic phases within 5 mm composite B (g).

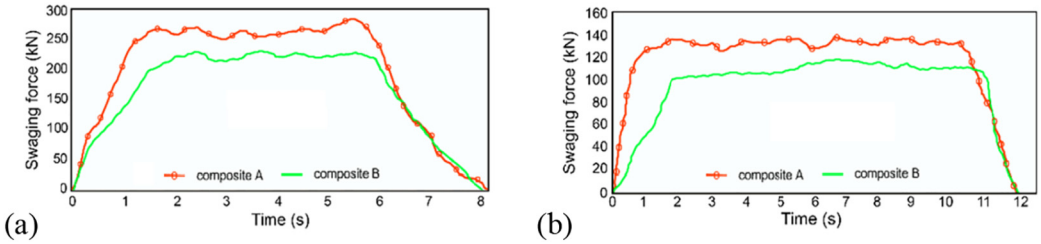

Fig. 4. Developments of swaging forces during swaging: 1st pass (a); 5th pass (b).

plasticity (elongation until fracture) for all the investigated diameters. As evident in Fig. 5, the highest UTS of almost 300 MPa was achieved for both the 10 mm composites, which points to significant work hardening during the swaging passes down to this diameter, however, the steep slopes of the stress-strain curves point to exhaustion of plasticity. During the swaging pass from 10 mm to 7.5 mm, the plasticity increased significantly and strength slightly decreased. The reasons for this behaviour were most probably the structure changes and occurring restoration induced primarily by the shear strain imposed via the radial movement of the dies (significant changes in plastic flow in this swaging pass can also be observed in Fig. 2) [30]. The curves for the 7.5 mm composites exhibited steep initial increase followed by a relatively steady elongation until fracture. Swaging down to 5 mm resulted in a decrease in plasticity and a slight decrease in UTS. The 5 mm samples exhibited fracture practically right after the initial increase (especially composite *A*), which points to a significant overall work hardening during this last swaging pass. Nevertheless, the comparison of all the stress-strain curves reveals decreasing work hardening intensity with decreasing composite diameter (the slope of both the 5 mm composites curves are the least steep). Given by the stacking sequence and the nature of the RS process, the Cu component has the major influence on the strength of the whole composite (primarily due to its higher volume fraction and generally higher strength) [25,31]. Increasing total imposed strain supports work hardening and strengthening for aluminium (as also discussed in Section 3.4), but plasticity increase for copper [32]. These factors were most probably the reasons for the slight UTS decrease for 5 mm composites, the cross-section areas of the Al wires within which decreased when compared to the larger composite diameters (Table 2). However, the structure changes induced by the energy accumulated by the effect of imposed strain – and elevated temperature in case of composite *B* – also contributed to the slight decrease in UTS and increase in plastic properties.

3.4. Structure observations

EBSD analyses revealed significant grain refinement and structure restoration occurring especially during the final swaging pass. Fig. 6a shows the grain size distribution within the Cu component of 6 mm composite *A*, while Fig. 6b depicts grain sizes for Cu within 5 mm composite *A*. The grain refinement during the last swaging pass is evident; the figures show the majority of the grains in the 6 mm sample to be of the size of around 2 μm, while the 5 mm sample Cu exhibited submicron grains; most of them had the size around 0.1 μm. On the other hand, processing to 5 mm at the elevated temperature led to slight grain growth of the grains within the Cu component due to the increased imposed energy as can be seen in Fig. 6c and d, the EBSD scan and corresponding grain size distribution for the Cu component of composite *B* in which are depicted. Nevertheless, the finest grains were observed within 5 mm composite *B*, the total imposed strain and elevated temperature for which provided advantageous conditions for recrystallization of Al. Fig. 6e depicts Al grains and their orientations within 5 mm composite *B*, while Fig. 6f shows grain size distribution within this component proving the significant grain refinement within the Al component leading to the formation of ultra-fine grained (UFG) structure. The grains in the Cu component were larger than in Al, however, various shades of the basic colours within the grains point to substructure development (formation of ultra-fine subgrains). This behaviour supports the aforementioned results of mechanical behaviour of the composite – the imposed strain provokes work hardening and significant grain refinement primarily within the Al component [32,33].

The 10 mm, 7.5 mm, 5 mm and original Al and Cu samples were further subjected to detection of Cu 220 and Al 200 diffraction peaks via neutron diffraction. The results of FWHM analyses supported the supposition of occurring recrystallization resulting in significant grain refinement and structure restoration during swaging to 5 mm drawn on the basis of EBSD analyses.

As evident in Fig. 7a, the structures of CP Cu and Cu within the 10 mm samples were comparable from the viewpoints of dislocation density and grain size. The data recorded for 7.5 mm composites Cu point to grain refinement and structure restoration within both the *A* and *B* samples, however, these phenomena were the most intense within 5 mm samples Cu, the FWHMs of which were the smallest. Mutual comparison of both the 5 mm samples showed the Cu

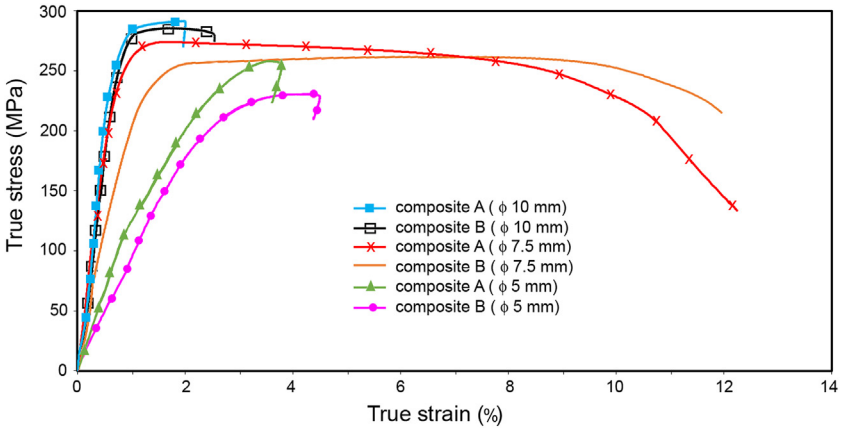

Fig. 5. Tensile test stress strain curves for various processing conditions.

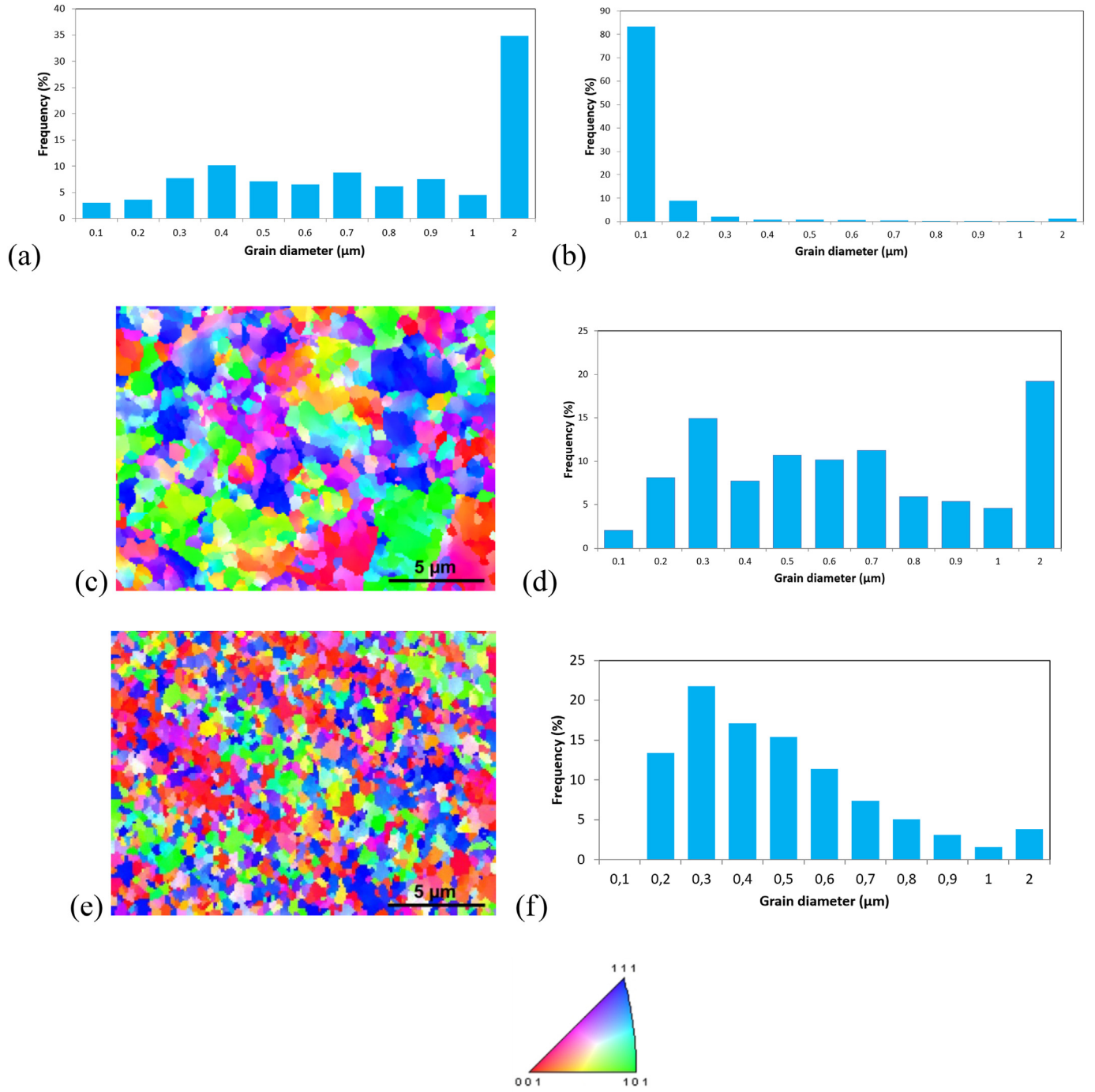

Fig. 6. Grain size distribution within 6 mm composite A Cu (a); grain size distribution within 5 mm composite A Cu (b); EBSD scan of 5 mm composite B Cu (c); grain size distribution within 5 mm composite B Cu (d); EBSD scan of 5 mm composite B Al (e); grain size distribution within 5 mm composite B Al (f).

structure of composite *B* to restore more intensively comparing to composite *A* (the effect of elevated temperature), which corresponds to the EBSD analyses. On the other hand, the Al FWHMs values depicted in Fig. 7b were comparable for all the composites. Due to the lower activation energy when compared to Cu, the imposed strain induced structure restoration primarily in this component. This was supported by the elevated swaging temperature of composite *B*. The comparison of identical diameters of both the composites shows that the FWHM value for composite *B* is slightly lower than for composite *A* in all cases, which points to a more significant restoration occurring within composite *B*.

3.5. Electric properties

The results of electric resistivity measurements depicted in Fig. 8 show this parameter to depend primarily on the deformation induced structure modifications. The dependence on the total imposed strain was non-linear – the highest values were recorded for the 10 mm diameters, while the lowest for the 7.5 mm ones. The significant resistivity decrease after swaging to 7.5 mm was most probably mainly caused by the occurrence of softening processes induced by the accumulated imposed strain (i.e. stored energy), which has been reported to support the development of restoration/recrystallization even at room

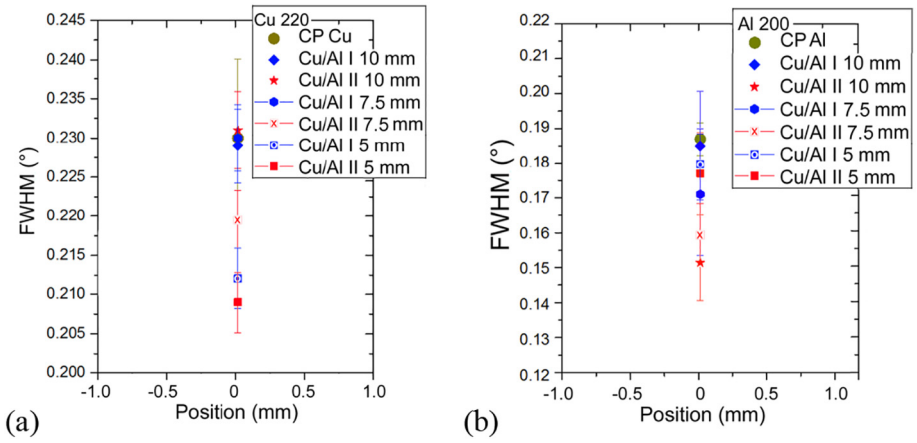

Fig. 7. Diffraction peak widths (FWHM) for Cu 220 (a) and Al 200 (b).

temperature processing [32,34]; work hardening, twinning, and formation of intermetallics has been reported among the structural phenomena deteriorating the electric properties [35,36]. The latter affected especially the composites subjected to higher reduction ratios; the resistivity of 6 mm and 5 mm composites *B* was higher than of 6 mm and 5 mm composite *A* also by the effect of intermetallic phases [37].

The substantial increase in electric resistivity after swaging to 6 mm was primarily the effect of work hardening (increase in dislocation density, deformation induced precipitation, deformation twinning, etc.), whereas the subsequent notable decrease in resistivity occurring after swaging to 5 mm was the primary result of the high reduction ratio supporting softening processes and structure restoration (Section 3.4), which eventually resulted in a decreased volume of structure obstacles for electrons flowing, i.e. decrease in resistivity.

Mutual comparison of the results for both the composites shows the resistivity to be higher for composite B for all the diameters except 7.5 mm, the tendency of the *A* and *B* composite values to invert can also be observed for 5 mm samples, the values for which were almost identical. This phenomenon can be attributed to the relatively low reduction ratio performed in the last swaging pass (Table 1), however, structure restoration, dislocations density and texture (grains orientations) development were the primary influencing factors. As proven by the results of microscopic analyses (Sections 3.1 and 3.4), both the 5 mm composites exhibited significant grain refinement, which was even supported by the elevated swaging temperature for composite *B* exhibiting the formation of a large amount of new ultra-fine grains, the boundaries of which act as obstacles for the movement of electrons and consequently slightly increase the electric resistivity (together with the effect of intermetallics development).

Nevertheless, the new boundaries did not affect the electric properties as significantly as work hardening; the resistivity for the restored UFG structures of 5 mm composites was lower than for the hardened structures of 6 mm ones. On the other hand, the 5 mm values were slightly higher than for 7.5 mm composites also featuring structure restoration, but larger grain size and thus lower fraction of grain boundaries [38]. The advantage of the 5 mm samples over the 7.5 mm ones is primarily in the mechanical properties, as documented e.g. in Section 3.3.

The comparison of the results with the previous study of a similar composite with inverted stacking sequence [25] shows that the dependence of electric resistivity on composite diameter has identical increasing/decreasing tendency for both the sequences, however, the changes in the values were more substantial in this study. One of the main influencing factors is the volume fraction of Cu within the composite – having better conductivity than Al, increased Cu content within the composite increased its overall conductivity. Also by this reason, the conductivity increased with increasing cross-sectional volume fraction of Cu, as depicted in Table 2. Moreover, the preferential axial plastic flow during swaging influencing orientations of the structural units (texture) advantageously corresponded to the direction of the electrons flow.

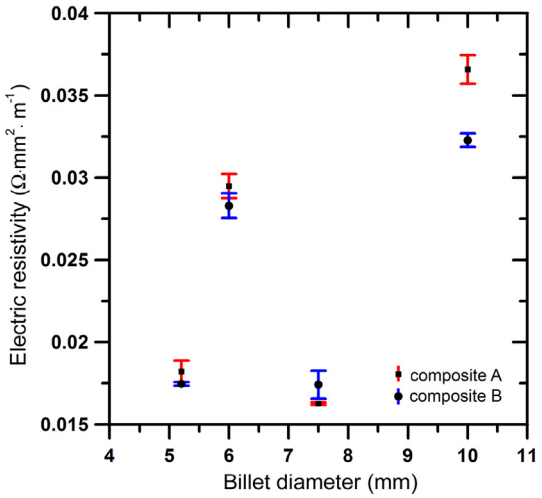

Fig. 8. Dependence of electric resistivity on swaged-composite diameter.

4. Conclusions

The presented research focused on the investigation of innovative 5 mm Cu/Al clad composite wires with unique sequencing successfully produced by rotary swaging at 20 °C and 250 °C. Both the Al and Cu 5 mm composites components exhibited recrystallized structures, especially the Al component exhibited sub-micron size UFG structure. Dynamic measurement of swaging forces showed the forces to decrease with decreasing composite diameter, however, deformation induced structure modification phenomena (i.e. precipitation, work hardening) imparted steady values for reduction ratios higher than ~1.5. Swaging at 20 °C imparted significant work hardening, increase in strength, and perfect bonding of the components. On the other hand, swaging at 250 °C facilitated plastic flow and structure restoration (i.e. plasticity increase), but supported the development of intermetallic phases at the interfaces within composites with high reduction ratios. Electric resistivity was generally higher for 250 °C composites due to the occurrence of intermetallics, and for hardened structures – it was the lowest for the restored structures of 7.5 mm and 5 mm composites (approx. 0.0165 $\Omega \cdot mm^2 \cdot m^{-1}$).

Acknowledgement

The paper was prepared with the support of the Ministry of Education, Youth and Sports (CANAM infrastructure of the NPI CAS Rez - project no. LM2015056, and infrastructure "Reactors LVR-15 and LR-0" - project no. LM2015074).

Data availability statement

The raw data required to reproduce this study cannot be shared at this time as the data are part of an ongoing study.

CRediT authorship contribution statement

Radim Kocich: Developed the KOMAFU S600 measuring system, Designed the unique sequencing and processing of the composites, Performed the swaging technology and evaluated the mechanical analyses and analyses of electric properties. **Lenka Kunčická:** Performed the swaging technology, Evaluated the mechanical analyses and analyses of electric properties, Helped with preparation of microscopic samples and evaluated microscopic analyses. **Petr Král:** Performed the preparation of microscopic samples, Performed the analyses, Evaluated the results and performed TEM analyses and their evaluation. **Pavel Strunz:** Performed the neutron diffraction analyses and evaluated their results.

References

[1] R. Kocich, A. Macháčková, L. Kunčická, F. Fojtík, Fabrication and characterization of cold-swaged multilayered Al-Cu clad composites, Mater. Des. 71 (2015) 36–47, https://doi.org/10.1016/j.matdes.2015.01.008.
[2] R.N. Yadav, V. Yadava, Experimental study of erosion and abrasion based hybrid machining of hybrid metal matrix composite, Int. J. Precis. Eng. Manuf. 14 (2013) 1293–1299, https://doi.org/10.1007/s12541-013-0176-x.
[3] C.-S. Kim, C. Randow, T. Sano (Eds.), Hybrid and Hierarchical Composite Materials, Springer International Publishing, Cham, 2015https://doi.org/10.1007/978-3-319-12868-9.
[4] L. Kunčická, T.C. Lowe, C.F. Davis, R. Kocich, M. Pohludka, Synthesis of an Al/Al_2O_3 composite by severe plastic deformation, Mater. Sci. Eng. A 646 (2015) 234–241, https://doi.org/10.1016/j.msea.2015.08.075.
[5] T.P.D. Rajan, B.C. Pai, Developments in processing of functionally gradient metals and metal–ceramic composites: a review, Acta Metall. Sin. 27 (2014) 825–838, https://doi.org/10.1007/s40195-014-0142-3.
[6] S.C. Tjong, Y.-W. Mai, Processing-structure-property aspects of particulate- and whisker-reinforced titanium matrix composites, Compos. Sci. Technol. 68 (2008) 583–601, https://doi.org/10.1016/j.compscitech.2007.07.016.
[7] M.U. Saeed, B. Li, Z. Chen, Z.M. Khan, A novel processing approach to produce microchannel embedded carbon-epoxy composites, J. Manuf. Process. 22 (2015) 26–33, https://doi.org/10.1016/j.jmapro.2016.01.007.
[8] R. Kocich, L. Kunčická, C.F. Davis, T.C. Lowe, I. Szurman, A. Macháčková, Deformation behavior of multilayered Al–Cu clad composite during cold-swaging, Mater. Des. 90 (2016) 379–388, https://doi.org/10.1016/j.matdes.2015.10.145.
[9] C. Sealy, Polymer composite combines novel properties, Mater. Today 20 (2017) 558–559, https://doi.org/10.1016/j.mattod.2017.11.008.
[10] L. Kunčická, R. Kocich, T.C. Lowe, Advances in metals and alloys for joint replacement, Prog. Mater. Sci. 88 (2017) 232–280, https://doi.org/10.1016/j.pmatsci.2017.04.002.
[11] A. Gueydan, B. Domengès, E. Hug, Study of the intermetallic growth in copper-clad aluminum wires after thermal aging, Intermetallics 50 (2014) 34–42, https://doi.org/10.1016/j.intermet.2014.02.007.
[12] R. Kocich, M. Greger, A. Macháčková, Finite element investigation of influence of selected factors on ECAP process, Metal 2010, 19th Int Metall Mater Conf, Tanger Ltd. 2010, pp. 166–171.
[13] A. Atrian, F. Fereshteh-Saniee, Deep drawing process of steel/brass laminated sheets, Compos. Part B Eng. 47 (2013) 75–81, https://doi.org/10.1016/J.COMPOSITESB.2012.10.023.
[14] P. Kazanowski, M.E. Epler, W.Z. Misiolek, Bi-metal rod extrusion—process and product optimization, Mater. Sci. Eng. A 369 (2004) 170–180, https://doi.org/10.1016/J.MSEA.2003.11.002.
[15] R. Kocich, L. Kunčická, P. Král, A. Macháčková, Sub-structure and mechanical properties of twist channel angular pressed aluminium, Mater. Charact. 119 (2016) 75–83, https://doi.org/10.1016/j.matchar.2016.07.020.
[16] I.-K. Kim, S.I. Hong, Effect of heat treatment on the bending behavior of tri-layered Cu/Al/Cu composite plates, Mater. Des. 47 (2013) 590–598, https://doi.org/10.1016/j.matdes.2012.12.070.
[17] X. Li, G. Zu, M. Ding, Y. Mu, P. Wang, Interfacial microstructure and mechanical properties of Cu/Al clad sheet fabricated by asymmetrical roll bonding and annealing, Mater. Sci. Eng. A 529 (2011) 485–491, https://doi.org/10.1016/J.MSEA.2011.09.087.
[18] R. Kocich, L. Kunčická, A. Macháčková, Twist Channel Multi-Angular Pressing (TCMAP) as a method for increasing the efficiency of SPD, IOP Conf Ser Mater Sci Eng, 63, , 2014, 12006. https://doi.org/10.1088/1757-899X/63/1/012006.
[19] L. Kunčická, R. Kocich, J. Drápala, V.A. Andreyachshenko, FEM simulations and comparison of the ecap and ECAP-PBP influence on Ti6Al4V alloy's deformation behaviour, Metal 2013, 22nd Int Met Mater Conf 2013, pp. 391–396.
[20] H.S. Arora, H. Singh, B.K. Dhindaw, Composite fabrication using friction stir processing - a review, Int. J. Adv. Manuf. Technol. 61 (2012) 1043–1055, https://doi.org/10.1007/s00170-011-3758-8.
[21] L. Li, K. Nagai, F. Yin, Progress in cold roll bonding of metals, Sci. Technol. Adv. Mater. 9 (2008), 23001. https://doi.org/10.1088/1468-6996/9/2/023001.
[22] R. Kocich, L. Kunčická, D. Dohnalík, A. Macháčková, M. Šofer, Cold rotary swaging of a tungsten heavy alloy: numerical and experimental investigations, Int. J. Refract. Met. Hard Mater. 61 (2016) 264–272, https://doi.org/10.1016/j.ijrmhm.2016.10.005.
[23] L. Kunčická, R. Kocich, C. Hervoches, A. Macháčková, Study of structure and residual stresses in cold rotary swaged tungsten heavy alloy, Mater. Sci. Eng. A 704 (2017) 25–31, https://doi.org/10.1016/j.msea.2017.07.096.
[24] X. Wu, Y. Zhu, Heterogeneous materials: a new class of materials with unprecedented mechanical properties, Math. Res. Lett. 5 (2017) 527–532, https://doi.org/10.1080/21663831.2017.1343208.
[25] R. Kocich, L. Kunčická, A. Macháčková, M. Šofer, Improvement of mechanical and electrical properties of rotary swaged Al-Cu clad composites, Mater. Des. 123 (2017) 137–146, https://doi.org/10.1016/j.matdes.2017.03.048.
[26] L. Kunčická, R. Kocich, Deformation behaviour of Cu-Al clad composites produced by rotary swaging, IOP Conf Ser Mater Sci Eng, 369, , 2018, 12029. https://doi.org/10.1088/1757-899X/369/1/012029.
[27] A. Ghaei, A. Karimi Taheri, M.R. Movahhedy, A new upper bound solution for analysis of the radial forging process, Int. J. Mech. Sci. 48 (2006) 1264–1272, https://doi.org/10.1016/J.IJMECSCI.2006.06.002.
[28] E. Moumi, S. Ishkina, B. Kuhfuss, T. Hochrainer, A. Struss, M. Hunkel, 2D-simulation of material flow during infeed rotary swaging using finite element method, Procedia Eng. 81 (2014) 2342–2347, https://doi.org/10.1016/j.proeng.2014.10.331.
[29] H. Amani, M. Soltanieh, Intermetallic phase formation in explosively welded Al/Cu bimetals, Metall. Mater. Trans. B Process Metall. Mater. Process. Sci. 47 (2016) 2524–2534, https://doi.org/10.1007/s11663-016-0682-1.
[30] L. Kunčická, R. Kocich, P. Král, M. Pohludka, M. Marek, Effect of strain path on severely deformed aluminium, Mater. Lett. 180 (2016) 280–283, https://doi.org/10.1016/j.matlet.2016.05.163.
[31] S. Tao, Z. Shengdun, Y. Guanhai, L. Hongbao, Plastic forming behavior of axisymmetric bimetal products with rotary swaging, Eng. Sci. 11 (2013) 44–47.
[32] F.J. Humphreys, M. Hetherly, Recrystallization and related annealing phenomena, 2nd ed. Elsevier Ltd, Oxford, 2004.
[33] O. Engler, V. Randle, Introduction to Texture Analysis, Macrotexture, Microtexture, and Orientation Mapping, 2nd ed. Taylor and Francis Group, 2010.
[34] R. Kocich, J. Fiala, I. Szurman, A. Macháčková, M. Mihola, Twist-channel angular pressing: effect of the strain path on grain refinement and mechanical properties of copper, J. Mater. Sci. 46 (2011) 7865–7876, https://doi.org/10.1007/s10853-011-5768-1.
[35] A. Russell, K.L. Lee, Structure-property Relations in Nonferrous Metals, 1st ed. John Wiley & Sons, Inc., New Jersey, 2005.
[36] B. Verlinden, J. Driver, I. Samajdar, R.D. Doherty, Thermo-mechanical Processing of Metallic Materials, Elsevier, Amsterdam, 2007.
[37] T. Liu, Q. Wang, Y. Sui, Q. Wang, W. Ding, An investigation into aluminum – aluminum bimetal fabrication by squeeze casting, JMADE 68 (2015) 8–17, https://doi.org/10.1016/j.matdes.2015.10.072.
[38] L. Kunčická, R. Kocich, P. Strunz, A. Macháčková, Texture and residual stress within rotary swaged Cu/Al clad composites, Mater. Lett. 230 (2018) 88–91.